Applied Energy 212 (2018) 1589–1600

Contents lists available at ScienceDirect

Applied Energy

journal homepage: www.elsevier.com/locate/apenergy

Online state-of-health estimation for lithium-ion batteries using constant-voltage charging current analysis

Jufeng Yang[a,b], Bing Xia[b,c], Wenxin Huang[a], Yuhong Fu[b], Chris Mi[b,*]

[a] Department of Electrical Engineering, Nanjing University of Aeronautics and Astronautics, 29 Jiangjun Street, Nanjing, Jiangsu 211106, China
[b] Department of Electrical and Computer Engineering, San Diego State University, 5500 Campanile Drive, San Diego, CA 92182, USA
[c] Department of Electrical and Computer Engineering, University of California San Diego, 9500 Gilman Dr., La Jolla, CA 92093, USA

HIGHLIGHTS

- Derived the expression of CV charging current based on ECM.
- Introduced time constant of CV charging current to estimate battery SoH.
- Established a quantitative correlation between current time constant and battery SoH.
- Discovered that current time constant is a logarithmic function of fitted data size.
- Employed uncompleted CV charging data to estimate battery SoH.

ARTICLE INFO

Keywords:
Lithium-ion battery
State-of-health (SoH)
Constant-current constant-voltage (CCCV) charge
Equivalent circuit model (ECM)
Current time constant

ABSTRACT

Battery state-of-health (SoH) estimation is a critical function in a well-designed battery management system (BMS). In this paper, the battery SoH is detected based on the dynamic characteristic of the charging current during the constant-voltage (CV) period. Firstly, according to the preliminary analysis of the battery test data, the time constant of CV charging current is proved to be a robust characteristic parameter related to the battery aging. Secondly, the detailed expression of the current time constant is derived based on the first order equivalent circuit model (ECM). Thirdly, the quantitative correlation between the normalized battery capacity and the current time constant is established to indicate the battery SoH. Specifically, for the uncompleted CV charging process, the logarithmic function-based current time constant prediction model and the reference correlation curve are established to identify the battery capacity fading. At last, experimental results showed that regardless of the adopted data size, the correlation identified from one battery can be used to indicate the SoH of other three batteries within 2.5% error bound except a few outliers.

1. Introduction

Due to the high energy and power density, lithium-ion batteries have proved to be a promising candidate as the energy storage system in electric vehicles (EVs) and consumer electronics [1–3]. To ensure the safety and reliability of battery systems, the basic battery states, i.e., state-of-charge (SoC) [4,5], state-of-power (SoP) [6], and state-of-health (SoH) [7,8], should be monitored continuously by the battery management system (BMS). Hence, the accurate, robust and practical battery state estimation is one of the key functions of a BMS. However, batteries are sophisticated electrochemical devices with various nonlinear characteristics. It is difficult to estimate the above states with high accuracy and strong robustness. Especially for the SoH estimation, the complicated aging mechanism and the uncertain external conditions (such as temperature and load profile) make it a more challenging task [9–11].

1.1. Review of the literature

To describe the deterioration of the power and the energy capability of the battery, the quantitative definition of the SoH is generally based on the impedance growth and/or the capacity loss. Hence, the SoH estimation can be converted to the identification of the present impedance and/or capacity.

Abundant research work has been conducted to seek the accurate impedance identification, ranging from offline tests, such as active/passive impedance spectroscopy [12,13], to online estimation algorithms, such as extended Kalman filter (EKF) based and least squares

* Corresponding author.
E-mail addresses: nuaayjf@163.com (J. Yang), bixia@eng.ucsd.edu (B. Xia), huangwx@nuaa.edu.cn (W. Huang), YFU@mail.sdsu.edu (Y. Fu), cmi@sdsu.edu (C. Mi).

https://doi.org/10.1016/j.apenergy.2018.01.010
Received 21 August 2017; Received in revised form 30 December 2017; Accepted 3 January 2018

based methods [14–17].

The battery capacity can generally be determined by two groups of approaches: the model-based and the correlation-based techniques.

According to the employed battery model, the model-based techniques can be further classified into two categories, namely, the black box model-based and the equivalent circuit model (ECM)-based techniques. For the black box model-based techniques, artificial neural networks [18,19], support vector machine [20,21], sample entropy [22,23] and sparse bayesian modeling [24] are generally employed to estimate the capacity fade in batteries. The advantage of these approaches is that the exact knowledge of battery aging mechanism is not considered, and only external behaviors of battery (e.g., voltage, current, and temperature) are required. Therefore, they are relatively simple and straightforward. However, the accuracy of the black box model is closely dependent on the quantity and quality of training data, which requires extensive offline training investigations [25]. By contrast, the ECM describes battery behaviors through a series of specific electric elements such as impedance components and voltage sources. The battery capacity can be estimated alone or together with other model parameters (e.g. impedance parameters, open circuit voltage (OCV)) and SoC through a variety of filters or observers, such as EKF [26,27], H-infinity filter [28], and recursive least squares algorithm [29]. These methods can theoretically estimate the capacity and other parameters as precisely as the battery is modeled. However, it has to be noted that three disadvantages exist concerning this type of technique. Firstly, a sufficient time is required to ensure the estimated capacity converge to the stable value [26]. Secondly, the accuracy of the estimation results strongly depends on the precision of the battery model, while an accurate battery model can significantly increase the computational cost [30]. Thirdly, the cross interference terms among the estimated variables can also compromise the estimation performance in terms of the numerical stability and accuracy [31].

From the perspective of correlation-based techniques, the battery capacity is indirectly determined based on the specific characteristic parameter, and the mapping relationship between capacity degradation and the related parameter variation should be established in advance. Typically, there exists several methods to derive the characteristic parameter from the dynamic discharging process [32,33]. However, besides the aging state, the battery model parameters are generally changeable with SoC, temperature and C-rate of the load current under the operating condition [12], and the accuracy of SoH estimation will be reduced without considering these influences. Ref. [32] selected the solid electrolyte interphase (SEI) resistance to predict the battery remaining capacity by the appropriate correlation function. This approach was found to be insensitive to discharge C-rate and effective in estimating the battery remaining capacity. Specifically, the average SEI resistance with respect to the specific SoC range was utilized to reduce the influence of SoC. However, the battery parameters are generally identified online from dynamic operating conditions with a random SoC range. Thus, obtaining the average value covering the specific SoC range in practice is a challenging task. Ref. [33] developed a formula to determine the battery capacity based on the estimated diffusion capacitance. The temperature dependency of diffusion capacitance was considered to improve the robustness of the fitting function. Nonetheless, extensive laboratory investigations were required to obtain an accurate correlation. Some methods were developed based on the relaxation data after the current interruption. With this kind of methods, the battery capacity can be derived based on the change in the OCV before and after a driving event [34,35]. Since only the SoC-OCV correlation was employed as a characteristic parameter, which was nearly unchanged by the battery aging state, these methods enabled a high accuracy of capacity estimation over the battery lifetime. However, the long-time relaxation period is required for the precise OCV measurement, which is not suitable for real applications. Recently, many researchers have concentrated on predicting the battery capacity based on the characteristic parameter extracted from the constant-current constant-voltage (CCCV) charging data. One of the commonly used methods is based on the incremental capacity (IC) or the differential voltage (DV) analysis [36–38]. With this type of technique, the battery aging mechanisms (i.e., loss of lithium inventory and loss of active material) can be identified by analyzing the peaks on the IC or DV curve [39]. However, since all the peaks on the IC or DV curve lie within the plateaus of the OCV curve which is vulnerable to the measurement noise, it is difficult to identify the distinct peaks directly from the measured data set. Meanwhile, the IC and DV curves are generally derived from the pseudo or real OCV curve. It requires completely charging/discharging the battery with micro currents or recording the battery terminal voltage after a long-time relaxation process at SoC points covering the entire range. Both methods are time-consuming and thus are not suitable for the on-board application [39]. Ref. [40] established a quantitative correlation between battery capacity and IC peak value, and the support vector regression was employed to extract the IC peak value. Ref. [41] considered the normalized location interval of the DV curve as the characteristic parameter, and correlated it with the capacity loss. The improved center least squares method was employed to extract the DV curve. These approaches utilized the battery charging data directly to detect the battery capacity fading, and showed robust performances against the measurement noise and data size. It has to be noted that better results would be expected using the OCV curve to obtain IC and DV curves, instead of the charging data [39,42]. In addition, because of the extensive computational power required, the robust parameter extraction algorithm employed in these methods is generally not applicable for the on-board implementation. Besides the IC or DV based methods, Ref. [43] calculated the battery pack capacity by transforming the charging voltage curve during the constant-current (CC) charging period, and only simple mathematical calculations were needed. However, the authors made the critical assumption that the battery should experience a complete CC charging cycle, which rarely happens in real applications, especially in EVs. Ref. [44] used the voltage-capacity rate curve to identify the battery capacity, and the genetic algorithm was carried out to find the optimum transformation parameter. Nevertheless, the performance of the voltage-capacity rate curve is sensitive to the sampling frequency and the measurement noise [40,45]. Moreover, the adopted genetic algorithm is still complicated for the on-board applications. Different from the methods described above, Ref. [46] recognized the battery capacity loss according to the constant-voltage (CV) charging data. The simple mathematical function was proposed to simulate the battery current behavior during the CV charging period, and an obvious linear correlation between the model parameter and the battery capacity was exploited. Although the verification results show that the simulated CV current matches well with the experimental data, the parameters in the developed function had no explicit physical meaning. Besides, a complete CV charging period is required to determine the accurate battery capacity loss, which is infeasible from a practical point of view.

1.2. Contributions of the paper

In this paper, the battery capacity fading is detected through the dynamic characteristic of the charging current during the CV period. The main contributions of this paper are:

(1) The time constant of CV charging current is firstly introduced to indicate the battery aging state. Compared with the CV charging time, the current time constant is a more robust characteristic parameter related to the battery aging. Based on the employed ECM, the CV charging current is expressed in the recursive form to obtain the detailed expression of the current time constant.
(2) An online battery SoH estimation method is developed based on the quantitative correlation between the normalized battery capacity and the current time constant. Experimental results show that there exist a strong linear regression between the normalized battery

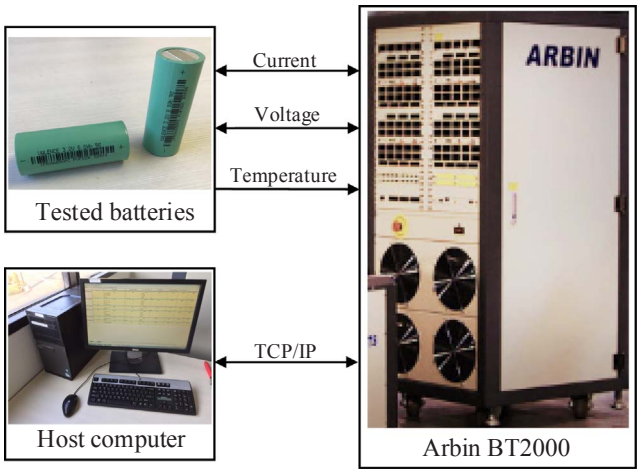

Fig. 1. Configuration of the battery test bench.

capacity and the current time constant. Besides, the correlation function extracted from one battery is able to evaluate the SoH of other three batteries with less than 2.5% absolute error except a few outliers.

(3) The uncompleted CV charging data is utilized to estimate battery SoH. Firstly, the logarithmic function-based prediction model is established to predict the reference current time constant. Then, the battery SoH can be estimated by substituting the reference time constant into the reference correlation curve. Comparison results demonstrate the superiority of the proposed method in terms of its robustness to data size.

2. Experimental tests and CV charging current analysis

2.1. Experimental setup

The battery test bench includes the tested batteries, an Arbin BT2000 cycle-based tester, and a host computer with MITS Pro software for experiment control and data storage, as shown in Fig. 1. Four lithium iron phosphate ($LiFePO_4$) IFR26650PC batteries from Valence are adopted under test. All four batteries, which are numbered from #1 to #4, are cycled with the same current excitations for comparison and validation. The specific parameters of the tested battery are listed in Table 1. The Arbin BT2000 cycle-based tester is used to charge and discharge the batteries and collect the test data. The voltage and current measurement ranges are 0–5 V and ± 100 A, respectively. The current measurement error in the battery tester is less than 0.05%, and the initial SoC can be obtained precisely from the test platform. Thus, it is feasible to assume that the accumulative battery capacity calculated through the recorded current can be considered as the reference value for comparison.

2.2. Test procedure

The test procedure, as shown in Fig. 2, is designed to generate rich excitations for the tested batteries. It mainly includes two parts: the aging and the characterization tests. All of the tests are conducted at

Table 1
Specifications of the tested battery.

Type	$LiFePO_4$
Nominal capacity	2.5 Ah
Nominal voltage	3.2 V
Charge cutoff voltage	3.65 V
Discharge cutoff voltage	2.0 V

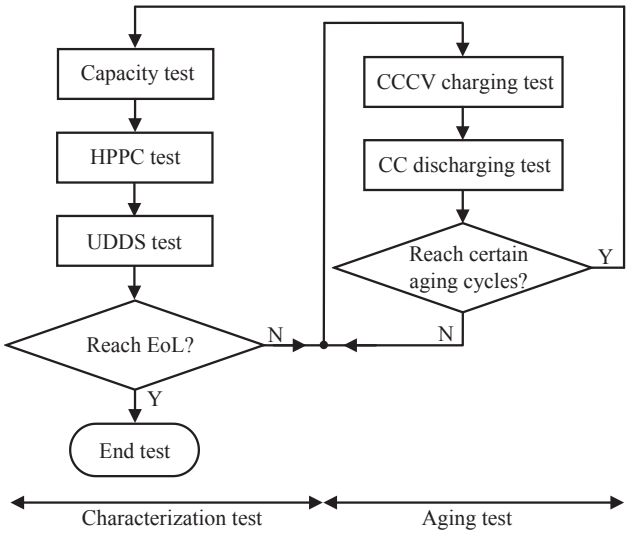

Fig. 2. Battery aging test procedure.

room temperature (the ambient temperature is 25 ± 2 °C), and the measured data sets, including current, voltage and temperature, are recorded with the sampling frequency (f_s) of 1 Hz.

The aging tests are conducted to explore the aging mechanism of the battery, e.g., loss of lithium inventory, loss of active material and Ohmic resistance increase [9]. It cycles until the battery reaches the end-of-life (EoL) condition (i.e., the battery's capacity reduces to 80% of its nominal capacity [32]). During each aging cycle, all four batteries are at 1C rate for CCCV charge and at 4C rate for CC discharge with no rest periods.

The characterization tests are performed periodically after certain aging cycles, which are aimed to extract battery parameters and acquire the corresponding variation tendency along with aging. As illustrated in Fig. 2, the characterization tests consist of a capacity test, a hybrid pulse power characterization (HPPC) test and an Urban Dynamometer Driving Schedule (UDDS) test. The battery capacity is derived from the capacity test comprising 5 charge-discharge cycles. Each cycle includes a 1/2C rate CCCV charge (CC-CV transition voltage: 3.65 V, cutoff current: 1/20C) and a 1/2C rate CC discharge processes. Finally, the battery capacity is calculated as the mean value of five cycles. The purpose of the HPPC test is to discharge/charge the battery to a certain SoC and excite the batteries dynamically. In the HPPC test, the battery is discharged/charged at a 5% SoC interval with 1/2C rate, and a 2 h rest is applied after each SoC variation operation. As shown in Fig. 3, the HPPC pulses include one pair of discharge and charge pulses. The magnitude and duration of each current pulse are 2C and 10 s, respectively. The rest period between each discharge and charge pulses (T_1 in Fig. 3) is 40 s, and the rest period after current pulses (T_2 in Fig. 3) is 60 s. The objective of the UDDS test is to validate the

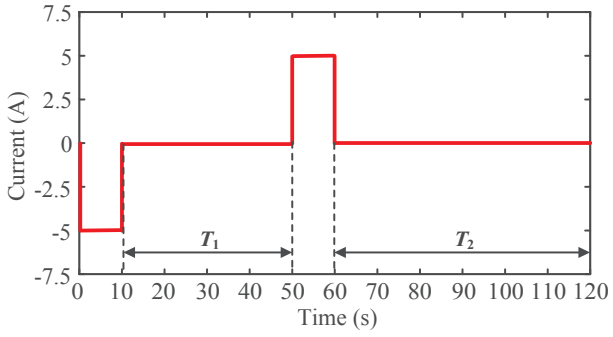

Fig. 3. The current profile of HPPC pulses.

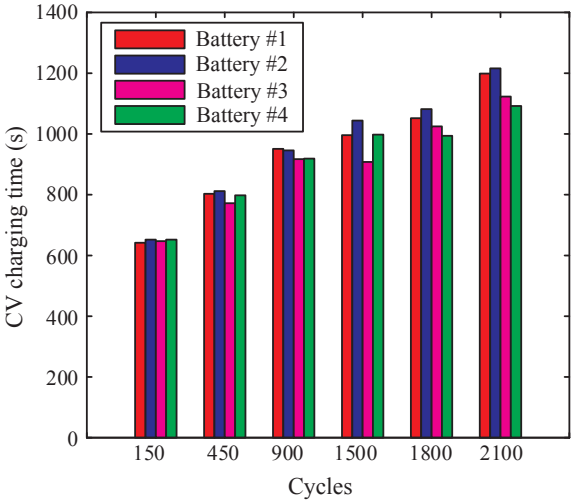

Fig. 4. Comparison of CV charging time for all four batteries.

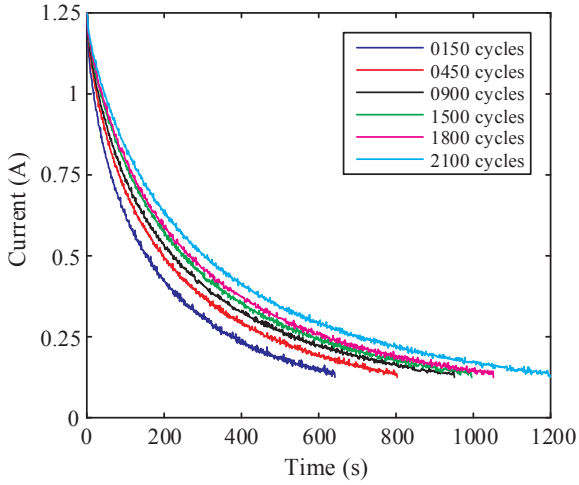

Fig. 6. Comparison of CV charging current after different aging cycles.

effectiveness of identified model parameters. In the UDDS test, the initial SoC is 90% and the cycle is repeated without rest until the SoC reaches 20%.

2.3. Preliminary CV charging current analysis

Fig. 4 shows the CV charging time of all four batteries after different aging cycles. For this study, all the CV charging data is extracted from the 5th cycle in the capacity test. It can be seen from Fig. 4 that the CV charging time (T_{CV}) generally possesses the increasing tendency with the growing aging cycles. It indicates that the battery aging state can be directly investigated from the CV charging time. In order to quantify the correlation between the battery capacity and T_{CV}, the normalized capacity (C_n) of battery #1 (battery #1 is considered as the reference battery in this paper) is plotted versus the corresponding T_{CV} in Fig. 5. The normalized capacity, as defined in (1), is adopted in this paper due to the inconsistency among different batteries.

$$C_n = \frac{C_{actual}}{C_{initial}} \tag{1}$$

where C_{actual} is the battery capacity obtained after each characterization test, and $C_{initial}$ is the battery capacity derived after the first characterization test.

It can be seen from Fig. 5 that C_n shows a monotonically decreasing relationship with T_{CV}. The solid line in Fig. 5 denotes the fitted linear correlation between C_n and T_{CV}. Fig. 5 demonstrates that with the complete CV charging process, the battery capacity can be obtained by substituting T_{CV} into the correlation established beforehand. However, it has to be noted that some batteries in the practical application cannot reach the cut-off current value due to the uncompleted charging process. In addition, the noise disturbance on the current measurement

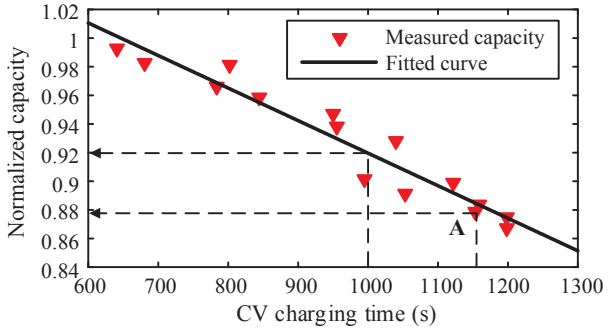

Fig. 5. Correlation between C_n and T_{CV} of battery #1.

may also cause the battery to finish the CV period earlier. Compared with the complete CV charging process, the shorter T_{CV} would be obtained from either of the above two scenarios, which in turn causes a significant SoH estimation error. For example, T_{CV} extracted after 2000 cycles of battery #1 is 1158 s, and the corresponding C_n should be 0.8782 (i.e., point A in Fig. 5). Nevertheless, if the CV charging process is terminated when T_{CV} equals 1000 s, the estimated C_n is 0.9195 when substituting T_{CV} into the correlation curve, as illustrated in Fig. 5. Thus, T_{CV} is highly sensitive to the external interference, and a more robust method is needed.

The CV charging current of battery #1 after different aging cycles are plotted in Fig. 6. It can be observed from Fig. 6 that with the growing aging cycles, the charging current reduces to the cut-off value at a slower variation rate, which in turn leads to a longer duration of the CV period. Since the current variation rate is closely associated with the relevant time constant, the current time constant (τ_I) for the CV charging period can thereby be adopted to investigate the battery aging state. Unlike T_{CV}, which should be obtained when the whole CV charging process is completed, τ_I can be extracted from the partial CV charging data, which will be discussed in great detail in Section 4.2. Hence, τ_I is a more robust characteristic parameter related to the battery aging, in comparison to the CV charging time.

3. Current time constant identification

3.1. Battery model and parameter identification

A proper battery model plays an important role in a high-performance BMS. Theoretically, the dynamic characteristic of a battery can be accurately described by the ECM with infinite resistor-capacitor (RC) networks [47]. However, this is an impractical battery model because of the heavy computational effort. Hence, considering the tradeoff between the model fidelity and computational complexity, the first order ECM is adopted in this paper.

The architecture of the first order ECM is shown in Fig. 7. It comprises a voltage source which represents the OCV, an Ohmic resistance (R_o) and an RC network ($R_p//C_p$). It should be noted that the above model parameters are generally represented as functions of SoC and temperature (T). Besides, the polarization resistance (R_p) and OCV also depend on the C-rate of the load current (C_I) [12] and hysteresis effect H [48], respectively, i.e.:

$$V_{OC} = V_{OC}(SoC,T,H), \quad R_p = R_p(SoC,T,C_I), \quad C_p = C_p(SoC,T),$$
$$R_o = R_o(SoC,T) \tag{2}$$

where C_p represents the polarization capacitance.

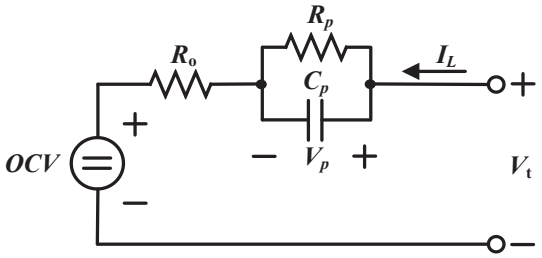

Fig. 7. The first order ECM.

The electrical behavior of the first order ECM can be expressed as

$$C_p\frac{dV_p}{dt}+\frac{V_p}{R_p}=I_L \tag{3}$$

$$V_{OC}+R_oI_L+V_p=V_t \tag{4}$$

where V_t represents the battery terminal voltage, V_p represents the voltage across the RC network, V_{OC} represents the OCV, and I_L is the load current, a positive value represents the charging scenario and a negative value represents the discharging scenario.

Based on (3) and (4), the transfer function of the first order ECM in the Laplace domain can be expressed as

$$H(s)=\frac{I_L(s)}{V_t(s)-V_{oc}(s)}=\frac{1+R_pC_ps}{R_o+R_p+R_oR_pC_ps} \tag{5}$$

By means of the z-transform, Eq. (5) yields

$$H(z)=\frac{I_L(z)}{V_t(z)-V_{oc}(z)}=\frac{z-\exp(-T_s/R_pC_p)}{R_o[z-\exp(-T_s/R_pC_p)]+R_p[1-\exp(-T_s/R_pC_p)]} \tag{6}$$

where T_s is the sampling period and is equal to 1 s in this paper.

This function can be rewritten as

$$I_{L,k}=I_{L,k-1}\theta_1+(V_{t,k}-V_{oc,k})\theta_2+(V_{t,k-1}-V_{oc,k-1})\theta_3 \tag{7}$$

where

$$\begin{aligned}\theta_1&=\exp(-T_s/R_pC_p)-(R_p/R_o)[1-\exp(-T_s/R_pC_p)]\\ \theta_2&=1/R_o\\ \theta_3&=-(1/R_o)\exp(-T_s/R_pC_p)\end{aligned} \tag{8}$$

The regression form of (7) can be expressed as

$$I_{L,k}=\varphi_k\theta \tag{9}$$

where

$$\begin{aligned}\varphi_k&=[I_{L,k-1}\quad V_{t,k}-V_{oc,k}\quad V_{t,k-1}-V_{oc,k-1}]\\ \theta&=[\theta_1\quad\theta_2\quad\theta_3]^T\end{aligned} \tag{10}$$

Among the parameters in (10), I_L and V_t can be measured directly, and V_{OC} can be obtained through a lookup table, which is normally identified by the HPPC test in advance. Besides, the impedance parameters (R_o, R_p and C_p) can be obtained by solving (9) with the discrete-time least squares (DT LS) method, which is widely implemented in the real applications. The algorithmic procedure of the DT LS method is not detailed in this paper, but can be referred to Ref. [49].

3.2. Expression of current time constant

In order to analyze the kinetic characteristic of the CV charging current, the detailed expression of the load current is needed.

Since V_p cannot be measured directly, the removal of V_p term from (3) and (4) is desired in order to obtain the current expression. Hence, substituting (4) into (3), the differential equation can be rewritten as

$$R_pI_L=C_pR_p\partial_tX+(V_t-V_{OC}-R_oI_L) \tag{11}$$

where vectors ∂_t and X are defined as

$$\partial_t=\left[\frac{dV_t}{dt}\quad\frac{dV_{OC}}{dt}\quad\frac{dR_o}{dt}\quad\frac{dI_L}{dt}\right],\quad X^T=[1\quad-1\quad-I_L\quad-R_o] \tag{12}$$

Since the battery terminal voltage is controlled constant during the CV period, the value of dV_t/dt can be considered as 0.

Considering (2), the variation of V_{oc} and R_o with respect to time can be further expressed as

$$\begin{cases}\frac{dV_{OC}}{dt}=\frac{\partial V_{OC}}{\partial SoC}\cdot\frac{dSoC}{dt}+\frac{\partial V_{OC}}{\partial T}\cdot\frac{dT}{dt}+\frac{\partial V_{OC}}{\partial H}\cdot\frac{dH}{dt}\\ \frac{dR_o}{dt}=\frac{\partial R_o}{\partial SoC}\cdot\frac{dSoC}{dt}+\frac{\partial R_o}{\partial T}\cdot\frac{dT}{dt}\end{cases} \tag{13}$$

In addition, Eq. (13) can be simplified considering the following assumptions:

(1) $dSoC/dt$ can be further express as $I_L/(3600C_{cap})$ (where C_{cap} is the capacity of the battery in Ah). Assuming that the battery is charged by a 2C constant current (generally less than this value in most applications [42], especially during the CV period), the value of $dSoC/dt$ is $I_L/(3600C_{cap})=2/3600=0.00056$, which is very small. Hence, $dSoC/dt\approx 0$ holds for normal charging conditions.
(2) Depending on the thermal management in the BMS, the battery temperature should be controlled in a proper range and the relevant variation should be slow, thus $dT/dt\approx 0$ can be obtained [50].
(3) Unlike the dynamic discharging process, the charging process is relatively simple and predictable. Hence, the model fidelity can be guaranteed by using the charging SoC-OCV relationship, and thus the hysteresis effect can be neglected, i.e., $dH/dt\approx 0$.

Based on the aforementioned analysis, $dV_{oc}/dt\approx 0$ and $dR_o/dt\approx 0$ hold for the charging condition, thus (11) can be rewritten as

$$\frac{dI_L}{dt}+\frac{R_p+R_o}{C_pR_pR_o}I_L=\frac{V_t-V_{OC}}{C_pR_pR_o} \tag{14}$$

where V_t-V_{OC} is considered as a constant item during one sampling period, and the impedance parameters (C_p, R_p and R_o) can be identified in advance through the algorithms mentioned above. Based on the general solution of the first order linear differential equation, I_L can be solved as

$$\begin{aligned}I_L=&I_{L,t_0}\exp\left(-\int bdt\right)\\&+\exp\left(-\int bdt\right)\int\left[(V_t-V_{OC})\exp\left(\int bdt\right)\Big/c\right]dt\end{aligned} \tag{15}$$

where I_{L,t_0} is the initial load current, $b=(R_p+R_o)/(C_pR_pR_o)$, and $c=C_pR_pR_o$. Defining $t_k=t_0$ and $t_{k+1}=t_0+T_s$, Eq. (15) can be simplified as

$$I_{L,k+1}=I_{L,k}\exp(-bT_s)+[(V_{t,k}-V_{OC,k})/d][1-\exp(-bT_s)] \tag{16}$$

where $I_{L,k}$ and $I_{L,k+1}$ represent the load current at time t_k and t_{k+1}, respectively, and $d=R_p+R_o$.

In the system expressed by (16), V_t-V_{OC} can be regarded as the system input, and the load current I_L is considered as the system response. If the system input is zero, the system response will decrease to 36.79% of its initial value when $T_s=1/b$. Similarly, for an increasing step input, if the initial current equals 0, the system response will reach 63.21% of its stable value when $T_s=1/b$. Hence, it can be concluded that the time constant for the CV charging current can be expressed as

$$\tau_I=\frac{1}{b}=\frac{C_pR_pR_o}{R_p+R_o} \tag{17}$$

3.3. Parametric sensitivity to sampling frequency

The sampling frequency is crucial for the performance of DT LS method. Without considering the limitation of on-board storage and

computation capabilities, the rapid sampling is normally desired so that the information on the fast dynamics can be captured [51]. However, the high sampling frequency will result in the eigenvalue being close to the unit circle in the z-domain, which can affect the stability for parameter identification [52]. Hence, the sensitivity of τ_I to f_s is worth investigating.

Generally, the location of the eigenvalue in the z-domain can be expressed as

$$z = \exp(\lambda T_s) \tag{18}$$

where λ is the eigenvalue of the system, and $|\lambda| = 1/\tau_I$.

Based on (18), the sensitivity of τ_I with respect to eigenvalue location in the z-domain is expressed as [49]:

$$S_z^{\tau_I} = \left| \frac{z}{\tau_I} \frac{\partial \tau_I}{\partial z} \right| = \frac{1}{|\lambda| T_s} = \tau_I f_s \tag{19}$$

It can be inferred from (19) that the higher sampling frequency yields higher sensitivity of identified τ_I. In a practical BMS, the sampling frequency can be 100 Hz, and τ_I identified after 2300 cycles is 233.8 s. Based on (19), the sensitivity can be as high as 23,380, which indicates that τ_I estimation is extremely sensitive to the eigenvalue location. Hence, to guarantee a good numerical stability, the sampling frequency in real application is recommended to limit to lower than a certain level.

3.4. Battery model verification

To verify the accuracy of the identified model parameters and the derived current expression during the CV charging period, the comparison results of battery #1 after 150, 1500 and 2200 cycles are shown in Fig. 8. Two evaluation criterions, including the Root Mean-Square Error (RMSE) and the *R-square* (R^2), are employed to evaluate the waveform similarity, as listed in Table 2. The definitions of RMSE and R^2 are described as

$$RMSE = \sqrt{\frac{1}{n} \sum_{k=1}^{n} (y_{\exp,k} - y_{est,k})^2} \tag{20}$$

$$R^2 = 1 - \frac{\sum_{k=1}^{n} (y_{\exp,k} - y_{est,k})^2}{\sum_{k=1}^{n} (y_{\exp,k} - \overline{y}_{\exp})^2} \tag{21}$$

where $y_{exp,k}$ and $y_{est,k}$ denote the experimental and the estimated values, respectively, $\overline{y}_{exp}$ is the mean value of the experimental data, and n is the data size.

It can be inferred from (20) and (21) that a lower RMSE (closer to 0) and a larger R^2 (closer to 1) indicate a better fitting performance. It can be concluded from Fig. 8 and Table 2 that the estimated current matches well with the measured charging current, which confirms that the extracted parameter set and the derived current expression can describe the transient behavior of the CV charging current with high fidelity.

4. SoH estimation based on the correlation between C_n and τ_I

4.1. Correlation identified from the complete CV charging data

Based on (16) and (17), τ_I can be identified from the CV charging data. Taking the data of battery #1 as the benchmark, C_n is plotted versus the corresponding τ_I in Fig. 9. It can be seen from Fig. 9 that C_n shows a monotonically decreasing relationship with τ_I. To quantitatively measure the degree of the linear relationship between C_n and τ_I, the correlation coefficient, or the Pearson product-moment correlation coefficient, is adopted in this paper. It can be described by (22) [38,53].

$$r_{xy} = \frac{\sum_{k=1}^{n} (x_k - \overline{x})(y_k - \overline{y})}{\sqrt{\sum_{k=1}^{n} (x_k - \overline{x})^2} \sqrt{\sum_{k=1}^{n} (y_k - \overline{y})^2}} \tag{22}$$

where x and y correspond to C_n and τ_I, respectively, and $\overline{x}$ and $\overline{y}$ represent the mean value of C_n and τ_I, respectively. The range of r_{xy} is $[-1, 1]$, where close to $+1$ indicates a strong positive correlation, close to -1 indicates a strong negative correlation, and close to 0 indicates a weak or totally missing correlation.

The correlation coefficient between C_n and τ_I of battery #1 is -0.9880, thus the linear function, as shown in (23), is employed to fit the obvious linear relationship between these two values.

$$C_n = a_1 \tau_I + b_1 \tag{23}$$

where a_1 and b_1 are the fitting function coefficients which can be

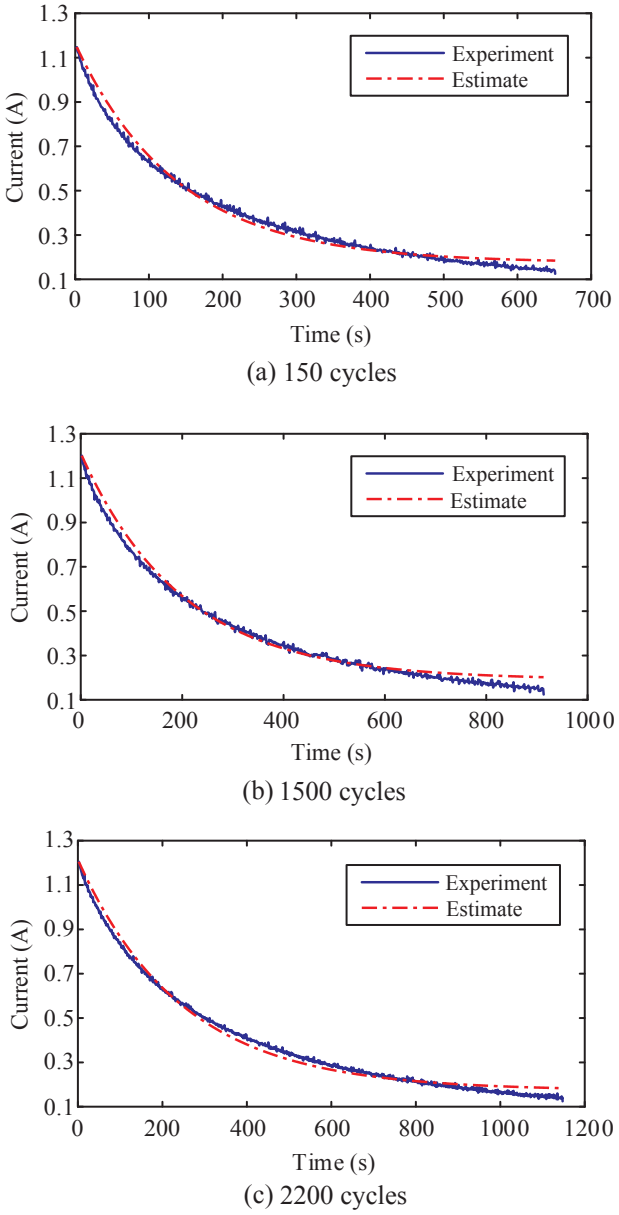

Fig. 8. Comparison between measured and estimated CV charging current after different cycles.

Table 2
Evaluation criterions of estimation performance after different cycles.

Cycles	RMSE	R^2
0150	0.02812	0.9855
1500	0.02812	0.9870
2200	0.02455	0.9905

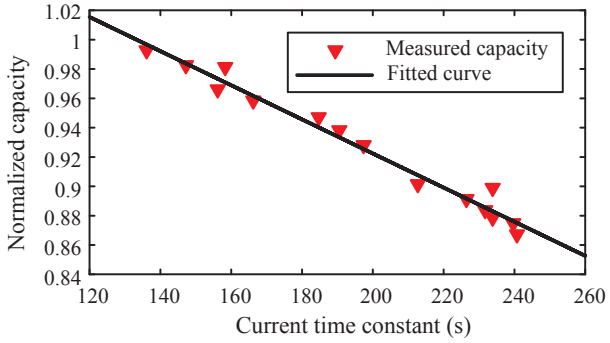

Fig. 9. Correlation between C_n and τ_I of battery #1.

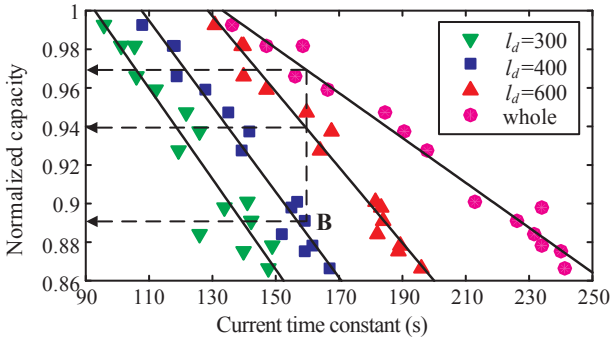

Fig. 11. Comparison of correlations between C_n and τ_I with respect to different l_d.

Table 3
Curve fitting results of battery #1.

a_1	b_1	RMSE	R^2
−0.001063	1.143	0.0113	0.9761

determined through curve-fitting method.

The fitted correlation curve is plotted as a solid line in Fig. 9. The detailed fitting function coefficients and two fitting quality criterions, including RMSE and R^2, are listed in Table 3.

It can be observed from Table 3 that the value of RMSE is small and the value of R^2 is close to 1, which indicates a good fitting performance. C_n and τ_I of all four batteries are plotted in Fig. 10. The solid line in the figure represents the correlation curve fitted through the data of battery #1, and the dotted lines give the error bound of 2.5%. It can be observed that most of the points are within the error bonds except one outlier, which confirms that the relationship between C_n and τ_I can be employed to indicate the battery SoH. In addition, it can be concluded that the linear relationship identified from the reference battery (battery #1) can also be used to evaluate the capacity degradation of the other three batteries. Hence, for the batteries from the same manufacturer, only the linear relationship of the reference battery should be established in advance, which can effectively reduce the testing effort.

4.2. Correlation identified from the partial CV charging data

4.2.1. Reference correlation curve selection

In practical applications, some batteries cannot reach the cut-off current value due to the uncompleted charging process or the measurement noise of the current sensors. Thus, only part of the CV charging current curve can be obtained in this case. Based on the existing research work [54,55], the identified time constant of the battery terminal voltage is not a constant value, but a variable as a function of open-circuit time. Similarly, the value of τ_I should also be a variable with respect to the length of CV charging data. Based on the data of

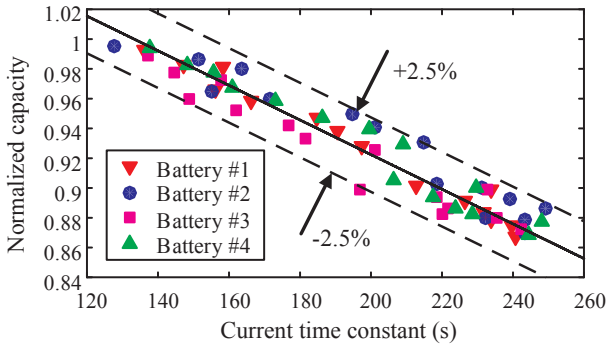

Fig. 10. Correlation between C_n and τ_I of all four batteries.

Table 4
Curve fitting results with respect to different l_d.

Data size	a_1	b_1	RMSE	R^2	Correlation coefficient
l_d = 300	−0.002348	1.218	0.01496	0.8912	−0.9440
l_d = 400	−0.00222	1.239	0.008814	0.9622	−0.9809
l_d = 600	−0.00196	1.252	0.007512	0.9731	−0.9865
Whole	−0.001163	1.155	0.00701	0.9761	−0.9880

battery #1, C_n is plotted versus the corresponding τ_I identified from the partial (the former 300, 400 and 600 sampling data) and the whole CV charging data in Fig. 11. In addition, the relevant correlation curves and the corresponding fitting results are shown in Fig. 11 and Table 4.

It can be observed from Fig. 11 that even in the same aging state, τ_I identified from the data with different lengths shows diverse values, which in turn leads to the various fitted correlation curves. Hence, applying τ_I corresponds to one specific data length (l_d) to the correlation curve with respect to other l_d can cause a significant SoH estimation error. For example, τ_I identified from the former 400 sampling data is 159.1 s, and the corresponding C_n should be 0.8912 (i.e., point B in Fig. 11). However, the estimated C_n is 0.9404 and 0.9701 when substituting τ_I into the correlation curve fitted from the former 600 sampling data and the whole data size, respectively, as illustrated in Fig. 11. The straightforward way to overcome this problem is to identify the correlation curve covering a wide range of l_d with a particular data length interval (Δl_d) in advance, then store them in the on-board microcontroller as a database. When τ_I of a specific l_d is identified, it can be put into the "C_n-τ_I database" to find a correlation curve with respect to a closest l_d. The accuracy of the estimated C_n depends on the selected Δl_d. The smaller Δl_d yields more details and thus the higher C_n estimation accuracy, whereas it requires more storage resources and offline identification efforts, especially for the battery with long CV charging period. Besides, it can be concluded from Table 4 that the correlation curve identified from the data with less l_d shows a worse fitting performance, which in turn leads to a larger SoH estimation error. An alternative method is to predict the specific τ_I ($\tau_{I,ref}$) corresponding to a predetermined longer l_d ($l_{d,ref}$), based on the uncompleted CV charging data. Then, the battery SoH can be estimated by substituting the predicted $\tau_{I,ref}$ into the reference correlation curve, which is identified from the data with size of $l_{d,ref}$. Although the correlation curve identified from the whole data size exhibits the best fitting performance, as illustrated in Table 4, it is impractical to employ it as the reference correlation curve, because the complete CV charging time cannot be obtained in advance. On the other hand, it can be concluded from Fig. 4 that the shortest complete CV charging time is slightly more than 600 s. Hence, the correlation curve identified from the former 600 sampling data is selected as the reference correlation curve in this paper.

4.2.2. Current time constant prediction

In order to predict $\tau_{I,ref}$, the functional relationship between τ_I and l_d

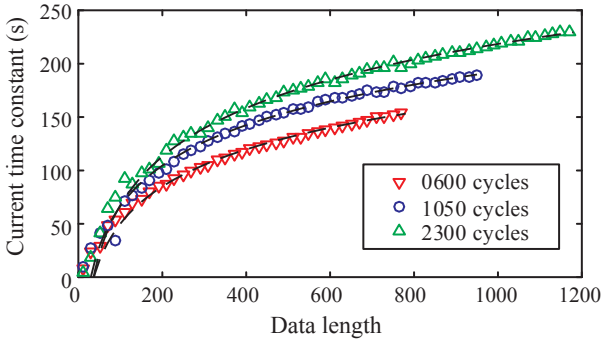

Fig. 12. Relationship between τ_I and l_d after different cycles.

should be determined firstly. Scatter plots of τ_I versus l_d after different cycles (600, 1050 and 2300 cycles) are shown in Fig. 12 to illustrate the relationship between these two sets of data.

It can be observed from Fig. 12 that τ_I increases with the increase of l_d. Considering the tendency of the related data, the fitting function as shown in (24) is adopted to quantitatively describe the relationship between τ_I and l_d [32].

$$\tau_I = a_2 \ln(l_d) + b_2 \tag{24}$$

where a_2 and b_2 are the fitting function coefficients. The fitting results, as shown in Fig. 12 (the dotted lines) and Table 5, demonstrate that the employed fitting function can accurately describe the increasing tendency of τ_I.

To evaluate the accuracy of the predicted $\tau_{I,ref}$ estimated from partial CV charging data, the identified fitting curves based on the first 300 and 400 sampling data after different cycles are given in Fig. 13. The actual τ_I points covering the former 800 sampling data are also plotted in Fig. 13. It shows that the identified curves match well with the actual points. This can also be observed in Table 6, where the relative errors between the predicted and the actual $\tau_{I,ref}$ are all less than 10% in six cases. In addition, compared with the predicted $\tau_{I,ref}$ based on the former 300 sampling data, the values obtained based on the former 400 sampling data have a lower overall error. This is because more fitted data points yield more information to predict the variation tendency of τ_I. Considering the accuracy of the predicted $\tau_{I,ref}$, at least 300 s of the CV charging period is required for the tested batteries.

4.3. Developed SoH estimation scheme

With the established reference quantitative relationship between C_n and τ_I, an online SoH (mainly on the battery capacity fading) estimation scheme is developed, as shown in Fig. 14. The measured battery voltage and current are recorded in the on-board storage component as soon as the charging process enters the CV charging mode. The recorded data sets are processed when the charging process is finished. If the recorded data size is no less than the selected $l_{d,ref}$ (e.g., 600 selected in this paper), $\tau_{I,ref}$ can be identified directly from the former sampling data with size of $l_{d,ref}$. Otherwise, the values of τ_I covering the former data sets with different lengths (e.g., $10, 20, \ldots, l_d$) identified firstly. Secondly, the quantitative correlation between τ_I and l_d (expressed as (24)) can be obtained through curve fitting method. Afterwards, $\tau_{I,ref}$ can be predicted by substituting $l_{d,ref}$ into the identified fitting function. At last,

Table 5
Curve fitting results after different cycles.

Cycles	a_2	b_2	RMSE	R^2
0600	48.33	−163.4	6.1466	0.9722
1050	61.27	−216.7	6.1371	0.9820
2300	71.07	−272.8	5.6040	0.9890

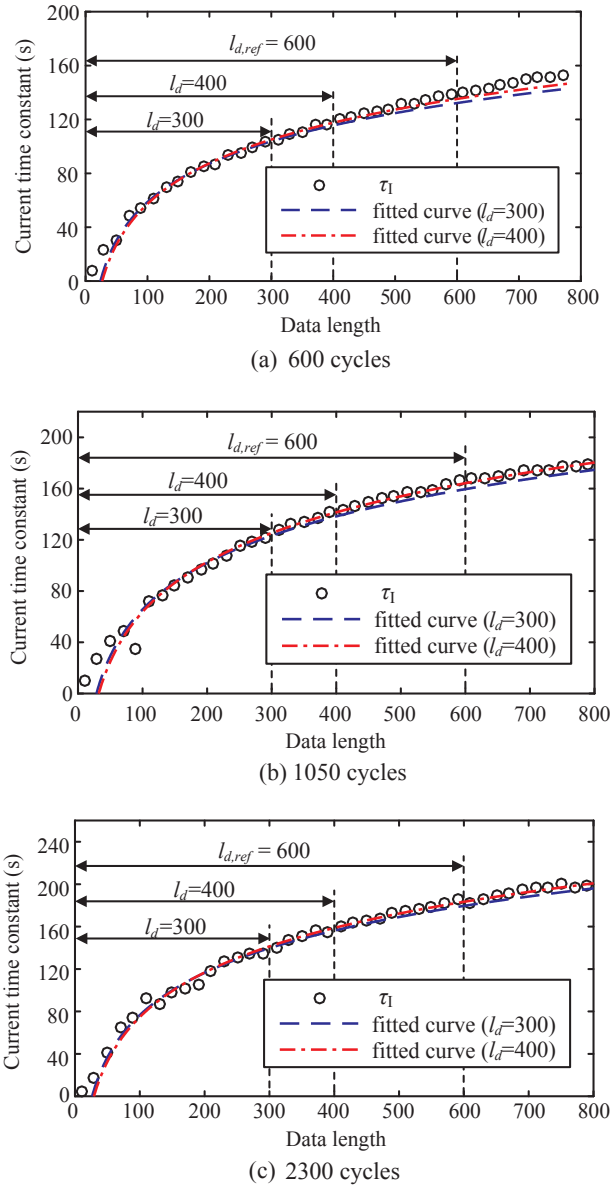

Fig. 13. Comparison between prediction curves and actual τ_I points after different cycles.

Table 6
$\tau_{I,ref}$ prediction results based on the different l_d.

Cycles	τ_{I,ref_actual}	$\tau_{I,ref\_predict}$ (l_d = 300)	Relative error (l_d = 300)	$\tau_{I,ref\_predict}$ (l_d = 400)	Relative error (l_d = 400)
0600	140.0 s	132.2 s	−5.571%	135.3 s	−3.357%
1050	167.7 s	159.6 s	−4.830%	164.2 s	−2.087%
2300	183.3 s	179.5 s	−2.073%	183.4 s	0.05456%

Note: τ_{I,ref_actual} is the actual $\tau_{I,ref}$ identified based on the former 600 sampling data, and $\tau_{I,ref\_predict}$ is the predicted $\tau_{I,ref}$ derived based on the prediction model.

the battery SoH can be derived using the correlation between C_n and $\tau_{I,ref}$, and the present battery capacity can be updated.

5. Verification and discussion

An online SoH estimation method is proposed in this paper, which is based on the analysis of load current during CV charging period. The developed method can be applied to the uncompleted CV charging process.

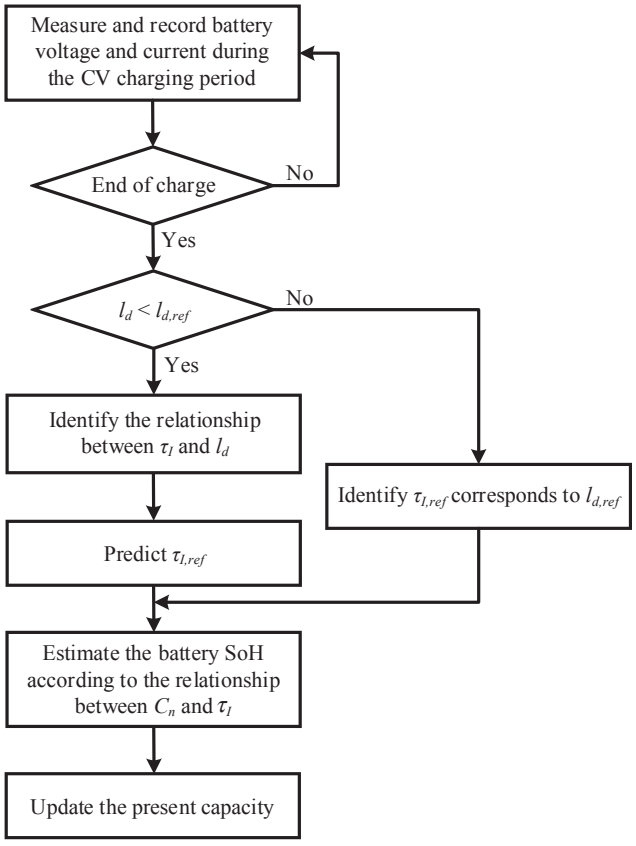

Fig. 14. The proposed online SoH estimation scheme.

Based on the reference correlation curve established upon the data from battery #1 and the logarithmic function-based $\tau_{I,ref}$ prediction model, all four batteries' SoH can be derived online from the CV charging data. Specifically, the definition of SoH is expressed as [33]:

$$\text{SoH} = \frac{C_{actual}}{C_{initial}} \times 100\% = C_n \times 100\% \tag{25}$$

Firstly, to assess the performance of the reference correlation curve established upon the data of battery #1, the SoH estimation results obtained from the former 600 sampling data ($l_{d,ref} = 600$) of all four batteries are listed in Table 7. It can be concluded from Table 7 that by using the reference correlation curve identified through the data of battery #1, the aging states of all four batteries can be estimated within 2.5% error bond except a few outliers. Hence, the battery SoH can be estimated by the reference correlation curve successfully. Furthermore, for the batteries from the same manufacturer, the correlation curve can be established by a reference battery in advance. Afterwards, the SoH of all the other batteries can be estimated when $\tau_{I,ref}$ is derived from the CV charging data.

Secondly, to evaluate the performance of the proposed method when l_d is less than $l_{d,ref}$, the SoH estimations based on the $\tau_{I,ref}$ prediction model (method 1) and "C_n-τ_I database" (method 2) are both conducted to make a comparison. The stored C_n-τ_I correlations are identified from the CV charging data ranging from the former 300 s ($l_d = 300$) to former 600 s ($l_d = 600$) with a resolution of 50 s ($\Delta l_d = 50$). Specifically, the former 320 s ($l_d = 320$) and former 420 s ($l_d = 420$) are employed to test the robustness of two methods in terms of data size. The comparison of SoH estimation results obtained from the former 320 and 420 sampling data of all four batteries are summarized in Tables 8 and 9, respectively. The results show that

(1) Compared with method 2, method 1 yields the lower overall SoH estimation error in both cases. It indicates the superiority of the $\tau_{I,ref}$ prediction model in terms of its robustness to the data size. With respect to method 2, better results will be obtained if the stored correlation curves are identified with shorter Δl_d. However, more storage resources and offline identification efforts are required, especially for batteries with the long-time CV charging period (e.g. more than 30 min for batteries in [46,56,57]).
(2) For both methods, the SoH estimated upon the longer l_d generally has a better performance, compared with the estimation results based on the shorter l_d. Based on the analysis in Section 4.2.2, the improved performance in method 1 is supposed to be caused by the more accurate $\tau_{I,ref}$ prediction results. For method 2, the improvement is supposed to be brought by the better fitting performance of the correlation curve, as has been discussed in Section 4.2.1.
(3) The SoH can be estimated by method 1 with less than 2.5% absolute error except a few outliers. Hence, based on the $\tau_{I,ref}$ prediction model, the battery SoH can be monitored by using the uncompleted CV charging data.

Table 7
SoH estimation results with $l_d = 600$ of all four batteries.

Battery #1			Battery #2		
SoH_{ref}	SoH_{est}	SoH_{err}	SoH_{ref}	SoH_{est}	SoH_{err}
98.15%	97.76%	−0.3981%	98.07%	96.71%	−1.359%
95.87%	96.39%	0.5234%	95.99%	96.34%	0.3485%
94.74%	93.92%	−0.8211%	94.91%	92.08%	−2.828%
93.77%	92.33%	−1.439%	93.01%	90.64%	−2.369%
92.78%	93.07%	0.2842%	90.31%	89.77%	−0.5444%
90.12%	89.68%	−0.4426%	89.23%	87.81%	−1.421%
89.12%	89.13%	0.01295%	88.57%	89.03%	0.4585%
87.82%	88.07%	0.2462%	87.02%	88.96%	1.940%
Battery #3			Battery #4		
SoH_{ref}	SoH_{est}	SoH_{err}	SoH_{ref}	SoH_{est}	SoH_{err}
98.86%	99.20%	0.3417%	99.46%	99.35%	−0.1130%
97.81%	97.95%	0.1451%	96.74%	96.58%	−0.1603%
95.27%	96.59%	1.323%	95.80%	95.03%	−0.7699%
92.53%	91.56%	−0.9770%	94.74%	94.90%	0.1566%
90.51%	89.49%	−1.017%	92.94%	90.92%	−2.018%
89.91%	88.97%	−0.9395%	90.51%	91.07%	0.5538%
89.33%	90.25%	0.9164%	88.19%	89.70%	1.516%
87.94%	86.12%	−1.821%	87.72%	86.45%	−1.270%

Note: SoH_{ref} are obtained based on the capacity measurement, and SoH_{est} and SoH_{err} are obtained based on the reference correlation curve.

6. Future work

In this paper, the simple first order ECM is adopted to characterize the battery behavior during the CV charging period. Besides, only $LiFePO_4$ batteries are tested and the charging condition is nearly constant through the aging test. Therefore, for the future work, some extensions to the employed model (e.g., the higher order ECM) will be considered to enhance the model performance. In addition, more experiments and further study are required to investigate the generality of the proposed method, including its potential to be used for different battery chemistries, charging protocols and operating temperatures.

7. Conclusion

An online SoH estimation method is proposed in this paper, which is based on the analysis of load current during CV charging period. According to the preliminary analysis of the battery test data, the time constant of CV charging current, which is derived based on the ECM, is considered as a robust characteristic parameter related to the battery capacity fading. The quantitative correlation between C_n and τ_I is established to indicate the battery SoH. Specifically, for the uncompleted

Table 8
SoH estimation results with l_d = 320 of all four batteries.

Battery #1					Battery #2				
SoH_{ref}	SoH_{est_1}	SoH_{err_1}	SoH_{est_2}	SoH_{err_2}	SoH_{ref}	SoH_{est_1}	SoH_{err_1}	SoH_{est_2}	SoH_{err_2}
98.15%	99.24%	1.082%	96.33%	−1.824%	98.07%	98.24%	0.1745%	95.41%	−2.655%
95.87%	98.28%	2.419%	95.07%	−0.7923%	95.99%	96.91%	0.9141%	94.62%	−1.376%
94.74%	95.56%	0.8257%	92.36%	−2.375%	94.91%	95.94%	1.031%	92.69%	−2.214%
93.77%	93.64%	−0.1323%	91.49%	−2.284%	93.01%	92.73%	−0.2856%	89.47%	−3.546%
92.78%	95.26%	2.478%	92.81%	0.02934%	90.31%	91.15%	0.8382%	88.96%	−1.350%
90.12%	90.04%	−0.07813%	87.93%	−2.189%	89.23%	89.90%	0.6685%	86.43%	−2.802%
89.12%	90.20%	1.085%	87.75%	−1.370%	88.57%	90.32%	1.747%	88.35%	−0.2163%
87.82%	88.93%	1.110%	86.73%	−1.091%	87.02%	89.75%	2.729%	87.29%	0.2675%
Battery #3					Battery #4				
SoH_{ref}	SoH_{est_1}	SoH_{err_1}	SoH_{est_2}	SoH_{err_2}	SoH_{ref}	SoH_{est_1}	SoH_{err_1}	SoH_{est_2}	SoH_{err_2}
98.86%	100.5%	1.641%	97.33%	−1.529%	99.46%	99.31%	−0.1487%	97.13%	−2.333%
97.81%	99.57%	1.767%	96.20%	−1.603%	96.74%	98.05%	1.308%	95.15%	−1.597%
95.27%	97.45%	2.188%	94.67%	−0.5999%	95.80%	96.56%	0.7582%	93.74%	−2.055%
92.53%	93.51%	0.9769%	91.23%	−1.299%	94.74%	95.80%	1.063%	92.58%	−2.158%
90.51%	91.52%	1.012%	88.57%	−1.938%	92.94%	92.29%	−0.6482%	90.08%	−2.857%
89.91%	87.78%	−2.127%	87.56%	−2.346%	90.51%	90.38%	−0.1354%	89.15%	−1.363%
89.33%	90.34%	1.007%	88.05%	−1.285%	88.19%	90.65%	2.462%	91.03%	2.846%
87.94%	85.81%	−2.132%	84.20%	−3.740%	87.72%	85.62%	−2.099%	82.38%	−5.340%

Note: SoH_{est_1} and SoH_{err_1} are obtained based on the $\tau_{I,ref}$ prediction model, and SoH_{est_2} and SoH_{err_2} are obtained based on the C_n-τ_I correlation curve with respect to l_d = 300.

Table 9
SoH estimation results with l_d = 420 of all four batteries.

Battery #1					Battery #2				
SoH_{ref}	SoH_{est_1}	SoH_{err_1}	SoH_{est_2}	SoH_{err_2}	SoH_{ref}	SoH_{est_1}	SoH_{err_1}	SoH_{est_2}	SoH_{err_2}
98.15%	98.56%	0.4072%	96.54%	−1.616%	98.07%	97.97%	−0.09717%	96.06%	−2.009%
95.87%	97.05%	1.184%	95.10%	−0.7621%	95.99%	96.25%	0.2590%	95.08%	−0.9134%
94.74%	95.11%	0.3717%	93.20%	−1.535%	94.91%	94.78%	−0.1376%	92.92%	−1.992%
93.77%	92.98%	−0.7898%	91.82%	−1.954%	93.01%	91.61%	−1.405%	89.58%	−3.432%
92.78%	94.27%	1.491%	92.81%	0.02712%	90.31%	90.40%	0.08593%	88.80%	−1.513%
90.12%	89.93%	−0.1905%	88.60%	−1.519%	89.23%	89.45%	0.2200%	86.66%	−2.572%
89.12%	89.51%	0.3883%	88.19%	−0.9307%	88.57%	88.52%	−0.0469%	86.78%	−1.790%
87.82%	89.24%	1.422%	87.15%	−0.6690%	87.02%	89.43%	2.407%	88.16%	1.145%
Battery #3					Battery #4				
SoH_{ref}	SoH_{est_1}	SoH_{err_1}	SoH_{est_2}	SoH_{err_2}	SoH_{ref}	SoH_{est_1}	SoH_{err_1}	SoH_{est_2}	SoH_{err_2}
98.86%	100.0%	1.141%	97.97%	−0.8868%	99.46%	99.49%	0.02794%	98.20%	−1.264%
97.81%	98.96%	1.158%	97.31%	−0.4918%	96.74%	97.14%	0.4014%	95.35%	−1.390%
95.27%	97.09%	1.820%	95.28%	0.01479%	95.80%	96.37%	0.5701%	94.21%	−1.588%
92.53%	92.37%	−0.1679%	90.56%	−1.971%	94.74%	95.35%	0.6095%	93.63%	−1.110%
90.51%	90.75%	0.2417%	88.57%	−1.943%	92.94%	91.80%	−1.143%	90.42%	−2.522%
89.91%	88.99%	−0.9155%	86.14%	−3.775%	90.51%	90.34%	−0.1729%	89.51%	−1.002%
89.33%	89.25%	−0.07653%	87.85%	−1.477%	88.19%	90.91%	2.724%	90.37%	2.183%
87.94%	86.86%	−1.081%	85.25%	−2.693%	87.72%	85.27%	−2.449%	83.93%	−3.796%

Note: SoH_{est_2} and SoH_{err_2} are obtained based on the C_n-τ_I correlation curve with respect to l_d = 400.

CV charging process, the reference correlation curve with respect to the specific data length is employed to estimate the battery SoH. Besides, the logarithmic function-based prediction model is identified from the partial CV charging data to predict $\tau_{I,ref}$. Four $LiFePO_4$ batteries are employed under test to verify the feasibility of the proposed method. The results demonstrate that the correlation coefficient between C_n and τ_I can reach −0.9880. Moreover, the correlation function extracted from one battery is able to evaluate the SoH of other three batteries with less than 2.5% absolute error except a few outliers, regardless of the adopted data size.

Acknowledgments

The authors would like to acknowledge the funding support from the China Scholarship Council (CSC) – China; the US DOE Graduate Automotive Technology Education (GATE) Center of Excellence; the National Science Foundation; and Nanjing Golden Dragon Bus Co., Ltd.

Appendix A.

Abbreviations and nomenclature

BMS	battery management system
CC	constant-current
CCCV	constant-current constant-voltage
CV	constant-voltage
DT LS	discrete-time least squares
DV	differential voltage
ECM	equivalent circuit model
EKF	extended Kalman filter
EoL	end-of-life
EV	electric vehicle
HPPC	Hybrid pulse power characterization
IC	incremental capacity
$LiFePO_4$	lithium iron phosphate
OCV and V_{OC}	open circuit voltage
RMSE	Root Mean-Square Error
SEI	solid electrolyte interphase
SoC	state-of-charge
SoH	state-of-health
SoP	state-of-power
UDDS	Urban Dynamometer Driving Schedule
a_1 and b_1	fitting function coefficients of the linear relationship
a_2 and b_2	fitting function coefficients of the logarithmic relationship
C_{actual}	Battery capacity obtained after each characterization test
C_{cap}	battery capacity
$C_{initial}$	Battery capacity obtained after the first characterization test
C_I	C-rate of the load current
C_p, R_p	Polarization capacitance and resistance
C_n	normalized capacity
H	Hysteresis effect
l_d	data length
Δl_d	data length interval
$l_{d,ref}$	reference data length
I_L	load current
r_{xy}	correlation coefficient between x and y
R^2	*R-square*
R_o	Ohmic resistance
T	temperature
T_1	rest period between each discharge and charge pulses in the HPPC test
T_2	rest period after current pulses in the HPPC test
T_s and f_s	sampling period and frequency
T_{CV}	CV charging time
V_p	voltage across the RC network
V_t	battery terminal voltage
λ	Eigenvalue of the system
τ_I	current time constant
$\tau_{I,ref}$	reference current time constant
τ_{I,ref_actual}	actual $\tau_{I,ref}$ identified based on the former 600 sampling data
$\tau_{I,ref\_predict}$	predicted $\tau_{I,ref}$ derived based on the prediction model
SoH_{est_1} and SoH_{err_1}	SoH estimation results based on the $\tau_{I,ref}$ prediction model
SoH_{est_2} and SoH_{err_2}	SoH estimation results based on "C_n-τ_I database"
SoH_{ref}	SoH estimation results based on the capacity measurement
SoH_{est} and SoH_{err}	SoH estimation results based on the reference correlation curve

References

[1] Mi C, Masrur MA, Gao DW. Hybrid electric vehicles: principles and applications with practical perspectives. John Wiley & Sons; 2011.

[2] Lu L, Han X, Li J, Hua J, Ouyang M. A review on the key issues for lithium-ion battery management in electric vehicles. J Power Sour 2013;226:272–88.

[3] Hosio S, Ferreira D, Goncalves J, van Berkel N, Luo C, Ahmed M, et al. Monetary assessment of battery life on smartphones. In: Proceedings of the 2016 CHI conference on human factors in computing systems; 2016. p. 1869–80.

[4] Zhang C, Wang LY, Li X, Chen W, Yin GG, Jiang J. Robust and adaptive estimation of state of charge for lithium-ion batteries. IEEE Trans Indust Electron 2015;62:4948–57.

[5] Lin C, Mu H, Xiong R, Shen W. A novel multi-model probability battery state of charge estimation approach for electric vehicles using H-infinity algorithm. Appl Energy 2016;166:76–83. [2016/03/15/].

[6] Sun F, Xiong R, He H, Li W, Aussems JEE. Model-based dynamic multi-parameter method for peak power estimation of lithium–ion batteries. Appl Energy 2012;96:378–86. [2012/08/01/].

[7] Shen WX, C CC, Lo EWC, Chau KT. Adaptive neuro-fuzzy modeling of battery

residual capacity for electric vehicles. IEEE Trans Indust Electron 2002;49:677–84.
[8] Ouyang M, Feng X, Han X, Lu L, Li Z, He X. A dynamic capacity degradation model and its applications considering varying load for a large format Li-ion battery. Appl Energy 2016;165:48–59. [2016/03/01/].
[9] Vetter J, Novák P, Wagner MR, Veit C, Möller KC, Besenhard JO, et al. Ageing mechanisms in lithium-ion batteries. J Power Sour 2005;147:269–81. [2005/09/09/].
[10] Berecibar M, Gandiaga I, Villarreal I, Omar N, Van Mierlo J, Van den Bossche P. Critical review of state of health estimation methods of Li-ion batteries for real applications. Renew Sustain Energy Rev 2016;56:572–87. [2016/04/01/].
[11] Jaguemont J, Boulon L, Dubé Y. A comprehensive review of lithium-ion batteries used in hybrid and electric vehicles at cold temperatures. Appl Energy 2016;164:99–114. [2016/02/15/].
[12] Waag W, Käbitz S, Sauer DU. Experimental investigation of the lithium-ion battery impedance characteristic at various conditions and aging states and its influence on the application. Appl Energy 2013;102:885–97. [2013/02/01/].
[13] Howey DA, Mitcheson PD, Yufit V, Offer GJ, Brandon NP. Online measurement of battery impedance using motor controller excitation. IEEE Trans Veh Technol 2014;63:2557–66.
[14] Plett GL. Extended Kalman filtering for battery management systems of LiPB-based HEV battery packs. J Power Sour 2004;134:277–92. [2004/08/12/].
[15] Wei Z, Meng S, Xiong B, Ji D, Tseng KJ. Enhanced online model identification and state of charge estimation for lithium-ion battery with a FBCRLS based observer. Appl Energy 2016;181:332–41. [2016/11/01/].
[16] He H, Xiong R, Guo H. Online estimation of model parameters and state-of-charge of LiFePO4 batteries in electric vehicles. Appl Energy 2012;89:413–20. [2012/01/01/].
[17] Wei Z, Lim TM, Skyllas-Kazacos M, Wai N, Tseng KJ. Online state of charge and model parameter co-estimation based on a novel multi-timescale estimator for vanadium redox flow battery. Appl Energy 2016;172:169–79. [2016/06/15/].
[18] Lin HT, Liang TJ, Chen SM. Estimation of battery state of health using probabilistic neural network. IEEE Trans Indust Inf 2013;9:679–85.
[19] Bai G, Wang P, Hu C, Pecht M. A generic model-free approach for lithium-ion battery health management. Appl Energy 2014;135:247–60. [2014/12/15/].
[20] Klass V, Behm M, Lindbergh G. A support vector machine-based state-of-health estimation method for lithium-ion batteries under electric vehicle operation. J Power Sour 2014;270:262–72. [2014/12/15/].
[21] You G-W, Park S, Oh D. Real-time state-of-health estimation for electric vehicle batteries: a data-driven approach. Appl Energy 2016;176:92–103. [2016/08/15/].
[22] Widodo A, Shim M-C, Caesarendra W, Yang B-S. Intelligent prognostics for battery health monitoring based on sample entropy. Expert Syst Appl 2011;38:11763–9.
[23] Hu X, Li SE, Jia Z, Egardt B. Enhanced sample entropy-based health management of Li-ion battery for electrified vehicles. Energy 2014;64:953–60. 2014/01/01/.
[24] Hu X, Jiang J, Cao D, Egardt B. Battery health prognosis for electric vehicles using sample entropy and sparse Bayesian predictive modeling. IEEE Trans Indust Electron 2016;63:2645–56.
[25] Waag W, Fleischer C, Sauer DU. Critical review of the methods for monitoring of lithium-ion batteries in electric and hybrid vehicles. J Power Sour 2014;258:321–39. [2014/07/15/].
[26] Wei Z, Tseng KJ, Wai N, Lim TM, Skyllas-Kazacos M. Adaptive estimation of state of charge and capacity with online identified battery model for vanadium redox flow battery. J Power Sour 2016;332:389–98. [2016/11/15/].
[27] Zou Y, Hu X, Ma H, Li SE. Combined state of charge and state of health estimation over lithium-ion battery cell cycle lifespan for electric vehicles. J Power Sour 2015;273:793–803. [2015/01/01/].
[28] Chen C, Xiong R, Shen W. A lithium-ion battery-in-the-loop approach to test and validate multi-scale dual H infinity filters for state of charge and capacity estimation. IEEE Trans Power Electron 2017. [pp. 1-1].
[29] Plett GL. Recursive approximate weighted total least squares estimation of battery cell total capacity. J Power Sour 2011;196:2319–31. [2011/02/15/].
[30] Hu X, Li S, Peng H. A comparative study of equivalent circuit models for Li-ion batteries. J Power Sour 2012;198:359–67. [2012/01/15/].
[31] Yang J, Xia B, Shang Y, Huang W, Mi CC. Adaptive state-of-charge estimation based on a split battery model for electric vehicle applications. IEEE Trans Veh Technol 2017. [pp. 1-1].
[32] Xiong R, Tian J, Mu H, Wang C. A systematic model-based degradation behavior recognition and health monitoring method for lithium-ion batteries. Appl Energy 2017;207:372–83. [2017/12/01/].
[33] Chen Z, Mi CC, Fu Y, Xu J, Gong X. Online battery state of health estimation based on Genetic Algorithm for electric and hybrid vehicle applications. J Power Sour 2013;240:184–92. [2013/10/15/].
[34] Kessels JTBA, Rosca B, Bergveld HJ, v d Bosch PPJ. On-line battery identification for electric driving range prediction. In: 2011 IEEE vehicle power and propulsion conference; 2011. p. 1–6.
[35] Einhorn M, Conte FV, Kral C, Fleig J. A method for online capacity estimation of lithium ion battery cells using the state of charge and the transferred charge. IEEE Trans Indust Appl 2012;48:736–41.
[36] Weng C, Feng X, Sun J, Peng H. State-of-health monitoring of lithium-ion battery modules and packs via incremental capacity peak tracking. Appl Energy 2016;180:360–8. [2016/10/15/].
[37] Li X, Jiang J, Wang LY, Chen D, Zhang Y, Zhang C. A capacity model based on charging process for state of health estimation of lithium ion batteries. Appl Energy 2016;177:537–43. [2016/09/01/].
[38] Berecibar M, Devriendt F, Dubarry M, Villarreal I, Omar N, Verbeke W, et al. Online state of health estimation on NMC cells based on predictive analytics. J Power Sour 2016;320:239–50. [2016/07/15/].
[39] Han X, Ouyang M, Lu L, Li J, Zheng Y, Li Z. A comparative study of commercial lithium ion battery cycle life in electrical vehicle: aging mechanism identification. J Power Sour 2014;251:38–54. [2014/04/01/].
[40] Weng C, Cui Y, Sun J, Peng H. On-board state of health monitoring of lithium-ion batteries using incremental capacity analysis with support vector regression. J Power Sour 2013;235:36–44. [2013/08/01/].
[41] Wang L, Pan C, Liu L, Cheng Y, Zhao X. On-board state of health estimation of $LiFePO_4$ battery pack through differential voltage analysis. Appl Energy 2016;168:465–72. [2016/04/15/].
[42] Gong X, Xiong R, Mi CC. A data-driven bias correction method based lithium-ion battery modeling approach for electric vehicles application. In: 2014 IEEE transportation electrification conference and expo (ITEC); 2014. p. 1–6.
[43] Wang L, Cheng Y, Zhao X. A $LiFePO_4$ battery pack capacity estimation approach considering in-parallel cell safety in electric vehicles. Appl Energy 2015;142:293–302. [2015/03/15/].
[44] Zheng Y, Lu L, Han X, Li J, Ouyang M. $LiFePO_4$ battery pack capacity estimation for electric vehicles based on charging cell voltage curve transformation. J Power Sour 2013;226:33–41. [2013/03/15/].
[45] Petzl M, Danzer MA. Advancements in OCV measurement and analysis for lithium-ion batteries. IEEE Trans Energy Convers 2013;28:675–81.
[46] Eddahech A, Briat O, Vinassa J-M. Determination of lithium-ion battery state-of-health based on constant-voltage charge phase. J Power Sour 2014;258:218–27. [2014/07/15/].
[47] Lee J, Nam O, Cho BH. Li-ion battery SOC estimation method based on the reduced order extended Kalman filtering. J Power Sour 2007;174:9–15. [2007/11/22/].
[48] Pérez G, Garmendia M, Reynaud JF, Crego J, Viscarret U. Enhanced closed loop state of charge estimator for lithium-ion batteries based on extended Kalman filter. Appl Energy 2015;155:834–45. [2015/10/01/].
[49] Xia B, Zhao X, de Callafon R, Garnier H, Nguyen T, Mi C. Accurate Lithium-ion battery parameter estimation with continuous-time system identification methods. Appl Energy 2016;179:426–36. [10/1/].
[50] Chiang Y-H, Sean W-Y, Ke J-C. Online estimation of internal resistance and open-circuit voltage of lithium-ion batteries in electric vehicles. J Power Sour 2011;196:3921–32. [2011/04/15/].
[51] Zheng Y, Ouyang M, Li X, Lu L, Li J, Zhou L, et al. Recording frequency optimization for massive battery data storage in battery management systems. Appl Energy 2016;183:380–9. [2016/12/01/].
[52] Garnier H, Mensler M, Richard A. Continuous-time model identification from sampled data: implementation issues and performance evaluation. Int J Control 2003;76:1337–57.
[53] Xia B, Shang Y, Nguyen T, Mi C. A correlation based fault detection method for short circuits in battery packs. J Power Sour 2017;337:1–10. [2017/01/01/].
[54] Pei L, Wang T, Lu R, Zhu C. Development of a voltage relaxation model for rapid open-circuit voltage prediction in lithium-ion batteries. J Power Sour 2014;253:412–8. [2014/05/01/].
[55] Yang J, Xia B, Shang Y, Huang W, Mi C. Improved battery parameter estimation method considering operating scenarios for HEV/EV applications. Energies 2017;10:5.
[56] Williard N, He W, Osterman M, Pecht M. Comparative analysis of features for determining state of health in lithium-ion batteries. Int J Prognost Health Manage 2013;4.
[57] Ramadass P, Haran B, Gomadam PM, White R, Popov BN. Development of first principles capacity fade model for Li-ion cells. J Electrochem Soc 2004;151:A196–203.